FIRST RESULTS FROM THE G0 PARITY VIOLATION EXPERIMENT CARRIED OUT AT JEFFERSON LABORATORY.

Louis Bimbot
for the **G0 collaboration**[1]

Institut de Physique Nucléaire, BP n° 1, F-91406 Orsay Cedex, France
e-mail : bimbotl@ipno.in2p3.fr

Abstract: The measurements were made at the Thomas Jefferson National Accelerator Facility, Newport News, VA (USA). Parity-violating asymmetries in elastic electron-proton scattering were determined over the range of momentum transfers Q^2 from 0.12 to 1.0 $(GeV/c)^2$, using a toroïdal spectrometer to detect the recoiling protons from a liquid hydrogen target. These asymmetries, arising from interference of the electromagnetic and neutral weak interactions, are sensitive to strange quark contributions to the currents of the proton. The results indicate non-zero, Q^2 dependent, strange quark contributions and provide new information beyond that obtained in previous experiments. Complementary measurements, planned for 2006, are described.

Keywords: *Experiment, asymmetry, parity violation, strange form factors.*

Introduction

The amplitude of the strange quark component in the description of the proton still has to be established. It cannot be evaluated from the electromagnetic interaction alone, but it can be accessed through electro-weak processes. The electro-weak interaction is smaller than the former one by orders of magnitude and requires special techniques to be observed and isolated. Parity violation is specific to the electro-weak interaction and forms the basis of the G0 experiment. The observables, the strange form factors of the proton, are extracted from asymmetry measurements for which many cancellations of experimental parameters permit access to a signal at the 10^{-6} level.

Several experiments are based on parity violation to determine the strange component of the nucleon: HAPPEX [**1**], PVA4 [**2**] and SAMPLE [**3**], but G0 [4] will be the largest investigation when both forward and backward angle measurements have been made, providing values of three form factors at three different Q^2. At the present stage of the experiment only the forward mode of detection has been used. The published results [5] don't give individual values of the electric and magnetic strange form factors of the proton and only trends can be deduced, as presented below.

[1] (see http://www.npl.uiuc.edu/exp/G0/)

At Nuppac'03, I gave a detailed presentation [6] of the set-up and its commissioning. Here I will only give short reminders of the physics and of the experimental approach but I will expose in detail the forward angle measurements, present the results, and summarize the goals and the status of the future backward angle experiment. This will include the description of the crucial parts of the data taking and of the analysis procedure as well as the technical developments required for the new measurements.

1. Physics goals

Parity violation in elastic electron scattering arises at leading order from the interference of the g and Z^0 exchange processes shown in Figure 1.

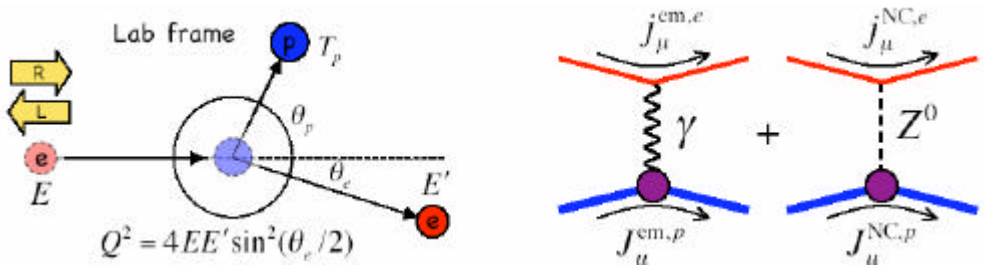

Figure 1. Diagrams for electron elastic scattering.
Left diagram summarizes the kinematics and right diagram represents the electromagnetic and electro-weak interactions, the interference of which makes the experiment possible.

The asymmetry of the reaction for the two helicity states of the beam can be expressed as:

$$A = -\frac{G_F Q^2}{4pa\sqrt{2}} \left\{ \frac{e G_E^g G_E^Z + t G_M^g G_M^Z - (1 - 4\sin^2 q_w)\, e' G_M^g G_A^e}{e (G_E^g)^2 + t (G_M^g)^2} \right\}$$

where:

$$\tau = \frac{Q^2}{4M_p^2}, \quad \varepsilon = \left(1 + 2(1+\tau)\tan^2\frac{\theta}{2}\right)^{-1}, \quad \text{and } \varepsilon' = \sqrt{\tau(1+\tau)(1-\varepsilon^2)}.$$

Q^2 is the squared four-momentum transfer ($Q^2 > 0$), G_F and α the usual weak and electromagnetic couplings, M_p the proton mass and q the laboratory electron scattering angle. G^γ_E and G^γ_M are the electromagnetic form-factors, G^z_E and G^z_M are the electroweak form-factors and G^e_A is the effective axial form-factor of the proton seen in parity-violating electron scattering. From the measurements of G^z_E, G^z_M and G^e_A and the knowledge of the electromagnetic form-factors of the proton and the neutron, it is possible to extract the ***s*** quark contribution (G^s_E and G^s_M) to the nucleon structure. This decomposition only relies on charge symmetry of the nucleon and on the assumption that only the light quark flavours contribute to these form factors. Finally the measured asymmetry can be expressed in terms of strange form factors:

$$A = h + x\, G^s_E + c\, G^s_M + f\, G^e_A$$

where h is the asymmetry known from neutron and proton form factors (for the G0 experiment h varies between -1 and -35 x10^{-6}) and x, c and f are coefficients depending on the kinematics.

Three asymmetry measurements are necessary to extract G^z_E, G^z_M and G^e_A - from which the strange form-factors can be deduced [**7**].

2. Experimental set-up

To undertake the experiment, specialized instrumentation has been set up in Hall C of Jefferson Laboratory, Newport News, Virginia, USA. A general view of the installation is shown in Figure 2.

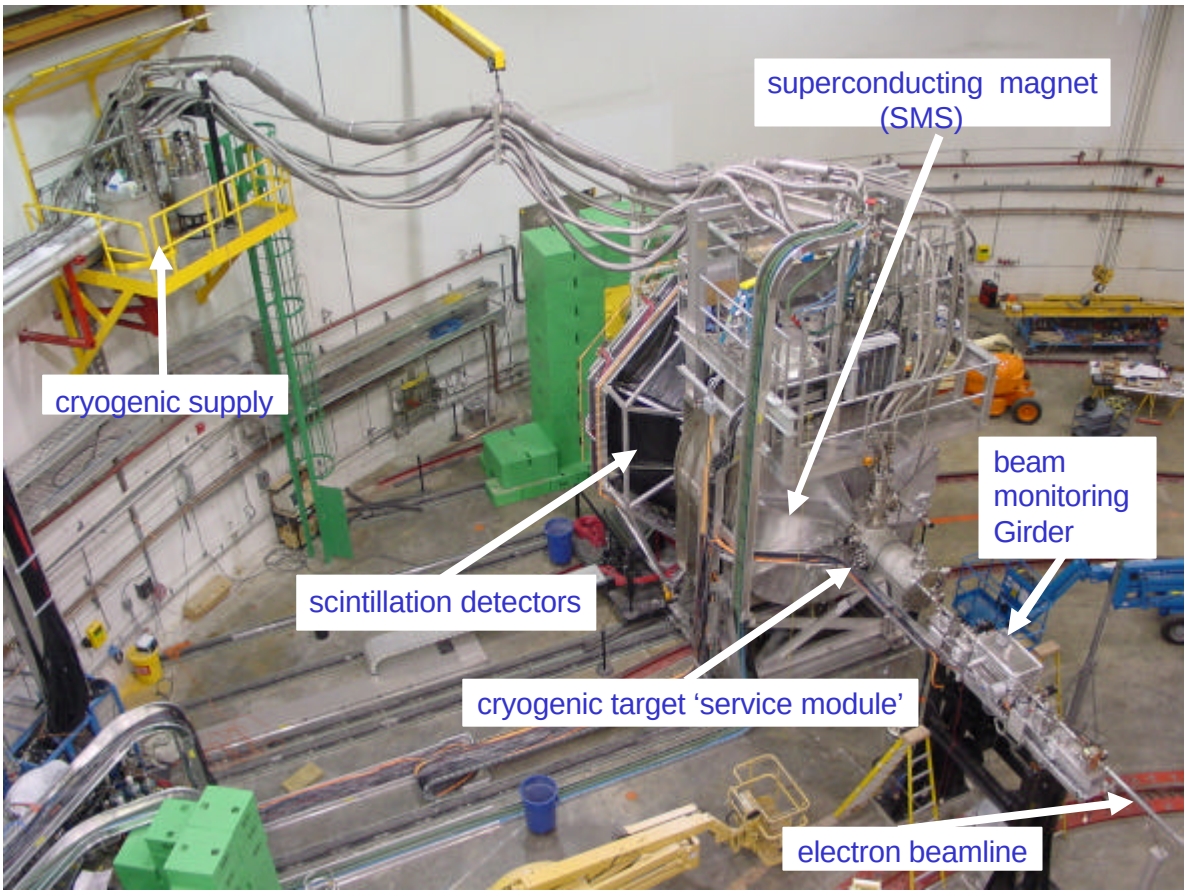

Figure 2. General view of the G0 set-up in Hall C.
The detection system is removable to allow other experiments in the same hall.

The main part of the detection system is the superconducting toroïdal magnetic spectrometer (SMS) specially designed and equipped to focus recoiling protons corresponding to a range of Q^2 transfer on to individual detectors made of scintillating plastic coupled to photo-multipliers and electronics. The beam energy is tuned at 3.03 GeV and the intensity is 40 μA, delivered in bunches of 32ns to enable time of flight measurements. The longitudinal polarization of the electrons is close to 74% and is reversed at a frequency of 30 Hz. With a current of 5000A in the SMS and the beam incident on a 20cm long liquid hydrogen target the detection covers the range of Q^2 from 0.12 to 1.0 $(\mathrm{GeV}/\mathbf{c})^2$ whereas the counting rate on individual counters is kept below 1 MHz due to dedicated shielding.

Two electronics systems have been developed independently by the American and French groups, covering one half of the detection each and providing complementary types of data. The French system giving a better time resolution has also been installed, in parallel with the North American one, on the detectors 14 and 15 of octants 1,3 5 and 7, to help for extracting different Q^2 zones from the data, as will be explained later in the analysis section. Typical ToF spectra are shown in Figure 3.

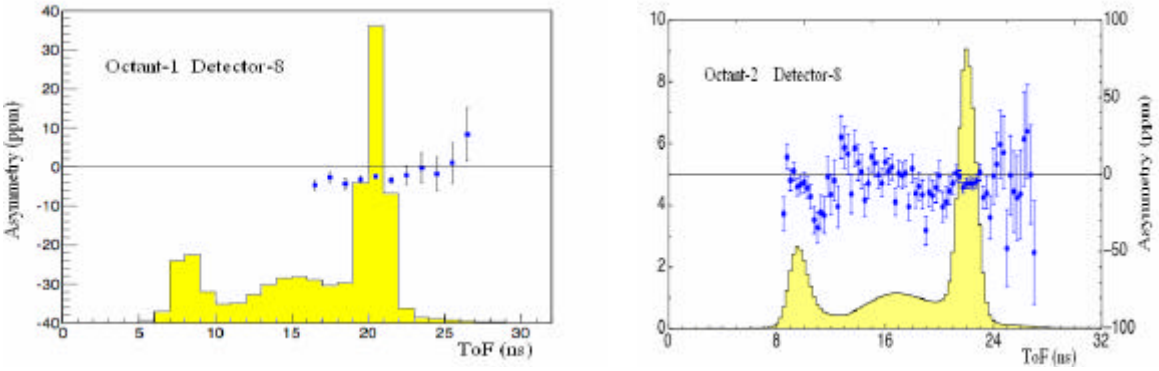

Figure 3: Typical time of flight (ToF) spectra from both electronics.
Octant 1 is equipped with North American electronics and Octant 2 with French electronics. The dots are representing the bin per bin asymmetry

Monitoring of the detector response is made with an additional electronics system, using fastbus ADC and TDC modules and working at low rate but in an event by event mode which enables correlation studies and checks on thresholds, amplifications and timing of the full experiment.

3. Data taking

3.1. Beam characteristics and controls

To use the ToF technique for particle identification, the accelerator had to be tuned in a special way with 32 nsec spacing between bunches. The mean intensity of 40µA, required for optimization of the data taking duration, corresponded to an increase by a factor of 16 of the charge per bunch. This tuning of the accelerator was a challenge for the technical team.

Table 1: Beam properties.
All the specifications required by the experiment were successfully met.

Beam Parameter	Achieved	"Specs"
Charge asymmetry	-0.14 ± 0.32 ppm	1 ppm
x position differences	3 ± 4 nm	20 nm
y position differences	4 ± 4 nm	20 nm
x angle differences	1 ± 1 nrad	2 nrad
y angle differences	1.5 ± 1 nrad	2 nrad
Energy differences	29 ± 4 eV	75 eV

The high accuracy of the measurements depended on a permanent control on the false asymmetry sources during whole experiment. Helicity correlated fluctuations were of most concern. It was then necessary to equip the beam line with specific tuning and control devices and to develop a sophisticated feedback system. The fluctuations were in beam position and angle at the target location, charge asymmetry in the incident beam and polarization. Table 1 gives a comparison of the specifications and the achieved performances.

3.2. Target study

The liquid target had to dissipate a huge amount of energy from the beam and it could cause boiling of the liquid H_2. A special magnetic device was installed to raster the beam position within a square of 4 by 4 mm. A detailed study has been carried out by varying the beam intensity in order to estimate target boiling effects [8]. It was established that 40 μA was still a safe value for operating during data taking. Some effects related with the shape of the liquid target container have been studied by moving slightly the target position.

3.3. Cross check measurements.

The beam quality and steadiness have insured safe data taking. Some measurements were dedicated to cross-checks and investigations for a full understanding of the critical points, such as background rates and asymmetries, leakage from the other halls, dead-time and Q^2 determination. It implied variations in the experimental parameters such as intensity, magnetic field in the SMS, target filling, etc. and has given a large set of data to evaluate various systematic uncertainties. As an example Figure 4 shows the investigations of beam leakage from the other halls.

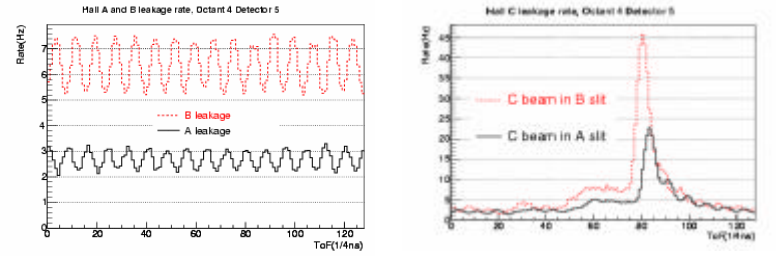

Figure 4. Investigation of leakage from other halls.

Three experiments can run simultaneously at JLab. with different beams adjusted on different slits but small leakages may happen to other halls. The figures are the ToF measured for different conditions: beam in hall A only, beam in hall B, hall C beam on slitA and hall C beam on slitB. These measurements were made to evaluate the correction to be applied for leakage from other halls.

4. Analysis procedure

4.1. Data were blinded during the analysis

The analysis of the data has been carried out by different people in parallel. To prevent influence from previous experimental data, a blinding factor was arbitrary introduced in the analyzing code and revealed in the ultimate stage before publication. The procedure is summarized in the chart of Figure 5.

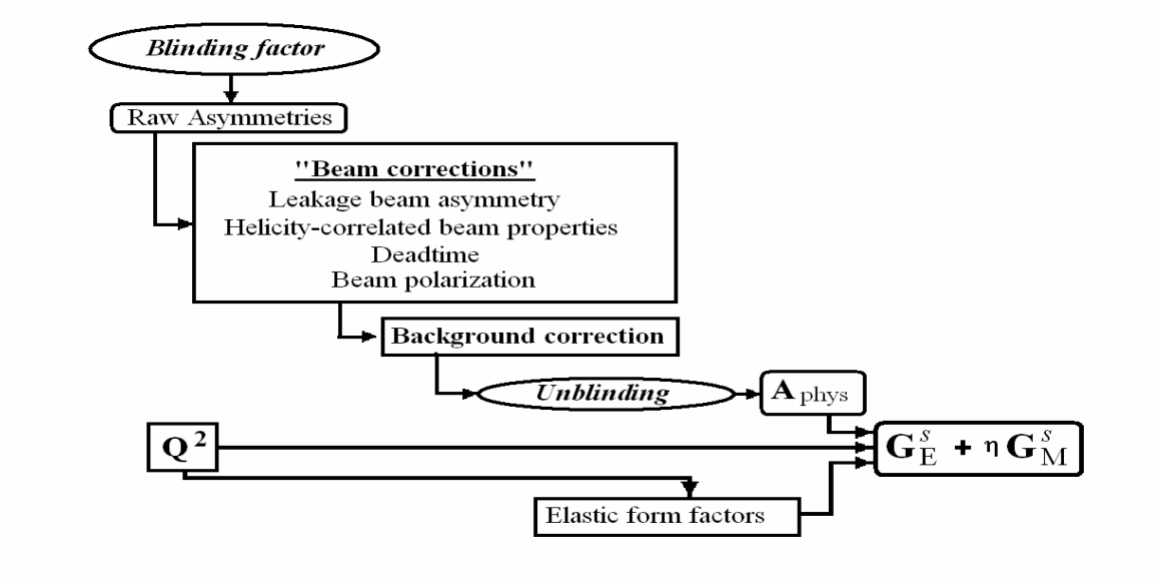

Figure 5. Summary of the analysis procedure.
Independent measurements were made for the asymmetry and Q^2 determination. Elastic form factors represent input from other experiments.

.

4.2. Q^2 determination

The spectrometer field integral and ultimately the Q^2 calibration ($\Delta Q^2/Q^2$ = 1%) was fine-tuned using the ToF difference between pions and elastic protons for each detector with dedicated measurements for which the detection conditions were adapted to provide full acceptance of the pions as well. The measurements were also compared to Monte-Carlo simulations [9]. Results and uncertainties are given below.

4.3. Elastic proton asymmetries

For each helicity state the ToF spectra are similar showing two peaks, one from recoiling protons from elastic scattering and one from pions. Between these peaks appear inelastic protons from different background contributions. The asymmetry measured bin-per-bin is also presented in Figure 6.

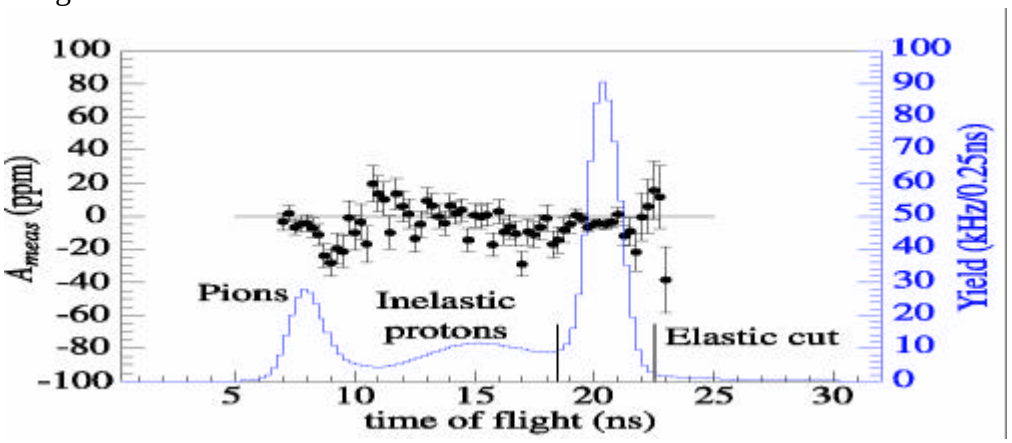

Figure 6: Detector 8: raw asymmetry A_{meas} (data points) and yield (histogram).
The zones of different physics processes are shown. The channel by channel asymmetry is represented by the full circles, with statistical error bars.

We use a logarithmic scale in Figure 7 to emphasize the different components and we visualize the different zones selected for preliminary analysis. The elastic asymmetry measured from the elastic cut is contaminated by background and leakage (grey part) contributions. To

study rates and asymmetries of these contaminations and to calculate a dilution factor four other 'cuts' are shown in the figure. The cut0 is dedicated to leakage studies [10] whereas cut1, cut2 and cut3 were used for background studies.

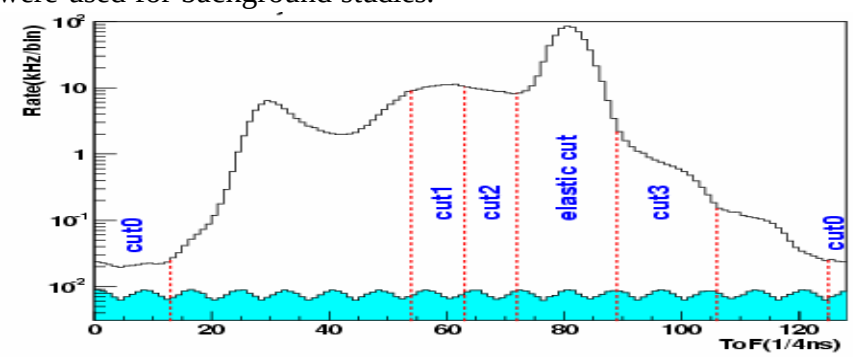

Figure 7: Different zones of the ToF spectrum used for background investigations. *The zone of cut0 is only accessible with the French electronics and has been crucial for the study of beam leakage yield and asymmetries*

4.4. Background subtraction and dilution factor

The best correction for the elastic asymmetry measurement is determined by fitting and/or interpolating the yield and asymmetry obtained from the ToF spectra.

Principle

The measured asymmetry has two components

$$A_{meas} = (1 - f)\, A_{el} + f\, A_{back}$$

where A_{el} is the raw elastic asymmetry, f is the background fraction and A_{back} the asymmetry of the background; in the actual analysis fits to the yield and asymmetry from the ToF spectra in the region of the elastic peak are used. The yield is typically modelled with a Gaussian elastic peak and a polynomial background. The asymmetry model comprises a quadratic background plus a constant. An example of the fits is given in Figure 8.

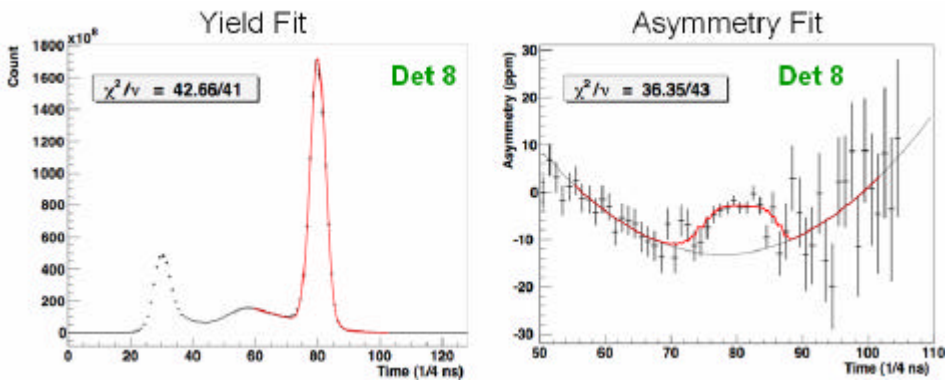

Figure 8: Results of the fitting procedure for yield and asymmetry. *For each detector, for elastic peak and background, yield and asymmetries are fitted either successively or simultaneously and final results are in agreement within error bars.*

Large positive $A_{background}$

The background asymmetry depends greatly on the Q^2 region of the measurement, as illustrated by Figure 9. For high number detectors it becomes positive with a maximum value of 45 ppm for detector 15.

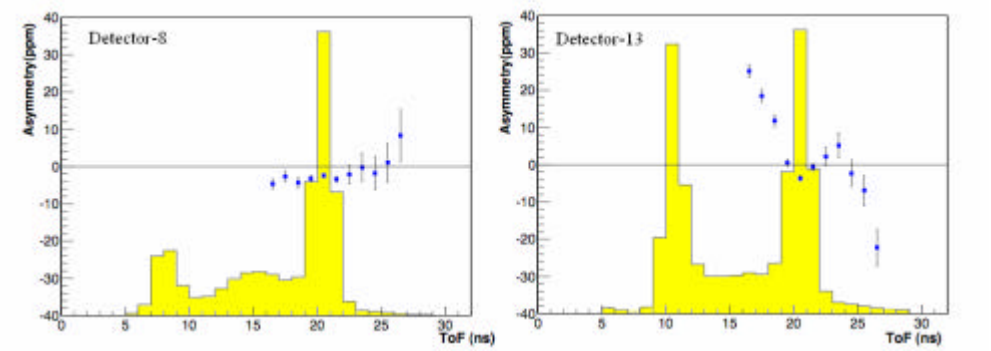

Figure 9: Background asymmetry changes with Q2.
In the case of detector 13, the background asymmetry is huge and varying across the elastic peak from positive to negative value

As substantiated by a Monte Carlo simulation, this positive asymmetry is caused by a small number of Λ and Σ weak-decay protons scattered inside the spectrometer [11]. The smooth variation of the region of positive asymmetries is tracked from detector 13 to 16 in Figure 10 and is presented with the results of simulations.

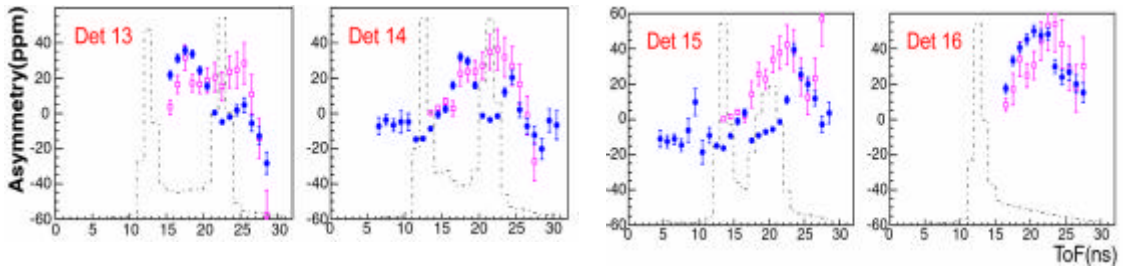

Figure 10: Positive background asymmetries.
The full circles are the measured values and the open circles correspond to a simulation of the asymmetry coming from in flight disintegration of hyperons. The high positive value is well reproduced.

4.5. Detector 14 {2 isolated Q^2 values}

The typical spectrum presents two peaks from protons corresponding to different Q^2. The higher Q^2, at lower ToF, corresponds to 1.0 $(GeV/c)^2$. The fitting procedure assumes different background shapes for the two regions separated by the vertical dotted line in Figure 11. A polynomial of degree 2 is used for the high ToF region but of degree 5 for the low ToF region, whereas the peak is always considered to be of Gaussian shape.
The results are presented in Figure 11.

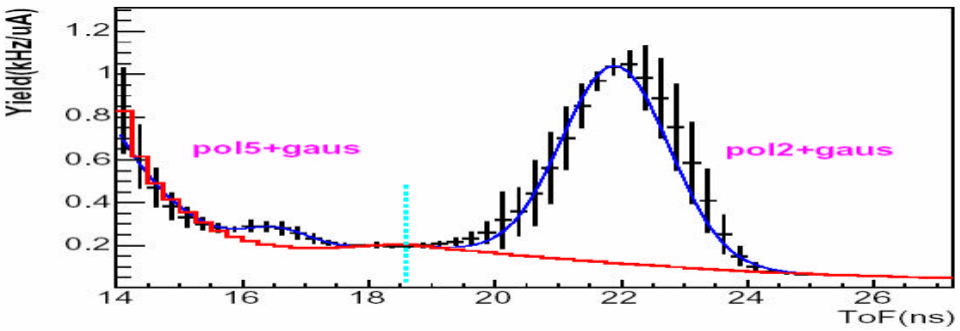

Figure11: Analysis of detector 14.
The background is a polynomial and the peaks are Gaussian.

4.6. Detector 15 {one peak - 3 zones of different Q^2 }

Due to kinematics the detector 15 is covering a large Q^2 range and the ToF peak corresponding to elastic scattering is wide. The analysis was done in considering three different windows associated with three different Q^2 values as shown in Figure12. The background study has required special attention and five different approaches have been developed [12] using either measurements at different magnetic fields, comparison with neighbouring detectors or extrapolation of fitting functions. The different results for the dilution factors agree within 10%, as reported in the table.

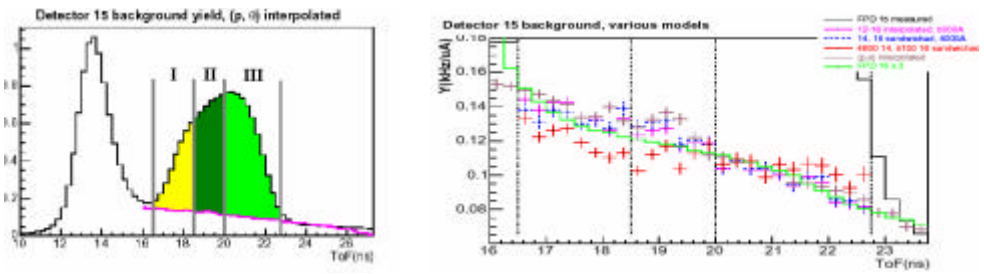

		Background fractions of 3 Q^2 bins, 5 methods				
ToF (ns)	$\langle Q^2 \rangle$ (GeV/c)^2	A	B	C	D	E
[16.5,18.5)	0.79	0.35	0.34	0.31	0.35	0.34
[18.5,20.0)	0.63	0.17	0.16	0.17	0.18	0.17
[20.0,22.75)	0.51	0.17	0.18	0.19	0.18	0.18

Figure 12: Dilution factor study for detector 15.
The top left figure shows the large elastic peak with the three zones defining the different Q^2 values given in the table. The top right picture is an illustration of the results from five different methods to estimate the background shape and magnitude under the peak. The dilution factor from each method is given in the table and agreement is within 10%, giving good confidence in the final result.

4.7. Deadtime corrections

All rates were corrected for dead-times of 10 – 15% on the basis of the measured yield dependence on beam current. The corresponding uncertainty in the asymmetry is of the order of 0.005 ppm.

4.8. Radiative corrections

Standard radiative corrections in the range of 1-3% determined by comparing simulations with and without radiation [13], were also applied to the asymmetries.

5. Published results

5.1. Asymmetries

The elastic asymmetries for the experiment, A_{phys} (A_{el} corrected for all effects described earlier) are presented in Table I. The statistical uncertainties include those from the background asymmetries. The systematic uncertainties are dominated by those from the background correction. This uncertainty is estimated from the range of elastic asymmetries generated from a variety of different background yields and asymmetry models. These models are bounded by the measured slopes of background yields and asymmetries on either side of the elastic peak

and varied continuously between these limits. The uncertainty in detector 15 is conservatively taken to be the difference between interpolated background asymmetries in successive detectors.

Table I: Asymmetries and uncertainties from the experiment.
The contributions to the systematic uncertainties are summarized in the right side part of the table. The first six are global, dead time is point-to-point and the background is a combination.

Q^2 (GeV^2)	A_{phys} (ppm)	ΔA_{stat} (ppm)	ΔA_{pt-pt} (ppm)	ΔA_{glob} (ppm)	f	A_{meas} (ppm)
0.122	-1.51	0.44	0.22	0.18	0.061	-1.38
0.128	-0.97	0.41	0.20	0.17	0.084	-1.07
0.136	-1.30	0.42	0.17	0.17	0.085	-1.34
0.144	-2.71	0.43	0.18	0.18	0.077	-2.67
0.153	-2.22	0.43	0.28	0.21	0.096	-2.46
0.164	-2.88	0.43	0.32	0.23	0.100	-3.13
0.177	-3.95	0.43	0.25	0.20	0.110	-4.47
0.192	-3.85	0.48	0.22	0.19	0.110	-5.01
0.210	-4.68	0.47	0.26	0.21	0.116	-5.73
0.232	-5.27	0.51	0.30	0.23	0.136	-6.08
0.262	-5.26	0.52	0.11	0.17	0.154	-5.55
0.299	-7.72	0.60	0.53	0.35	0.174	-5.40
0.344	-8.40	0.68	0.85	0.52	0.182	-3.65
0.410	-10.25	0.67	0.89	0.55	0.180	-1.70
0.511	-16.81	0.89	1.48	1.50	0.190	-5.80
0.631	-19.96	1.11	1.28	1.31	0.20	-9.74
0.788	-30.8	1.9	2.6	2.59	0.40	-12.66
0.997	-37.9	7.2	9.0	0.52	0.78	4.21

Systematic errors

Source	Uncertainty
Helicity-correlated beam parameters	0.01 ppm
Leakage beam	0.14 ppm
Beam polarization	1.0%
Ordinary radiative corrections	0.3%
Transverse polarization	0.01 ppm
Q^2	1%
Background correction	0.2 - 9 ppm
Deadtime	0.05 ppm

The results are presented in Figure 13. The curve labelled NVS, for No Vector Strange contribution, is obtained from a calculation using electromagnetic form factors from Kelly [14] and assuming no electroweak contribution ($G^s_E = G^s_M = 0$).

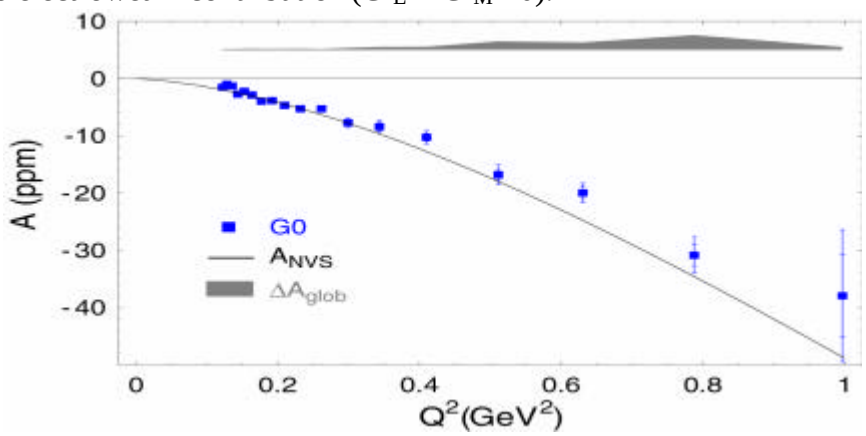

Figure 13: G0 measured asymmetries.

5.2. Form factors

The results in Figure 14 focused on the strange form factors. Only a linear combination of electric and magnetic can be extracted from the asymmetry, using the formula

$$G_E^s + \eta G_M^s = \frac{4\sqrt{2}\pi\alpha}{G_F Q^2}\frac{\mathcal{D}}{\varepsilon G_E^\gamma}\left(A_{phys} - A_{NVS}\right)$$

A_{NVS} is the 'no-vector strange' asymmetry.

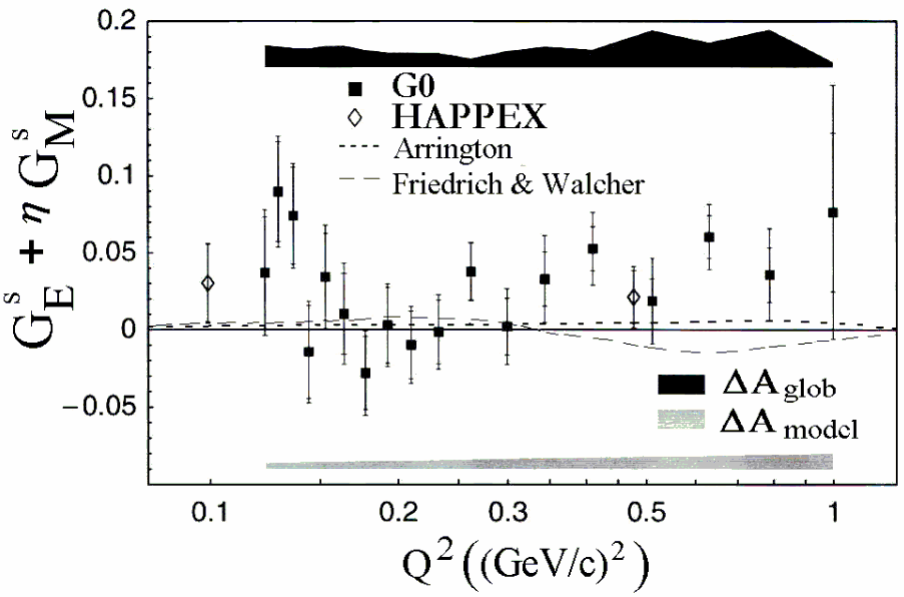

Figure 14. Linear combination $G_E^s + \eta\, G_M^s$.
Measurements from the G0 and HAPPEX experiments are plotted versus the momentum transfer Q^2. Note the log scale for Q^2 used to provide a better visual separation between the measurements. The black and grey bands represent correlated systematic uncertainties coming from the global experiment plus model ($A_{phys} - A_{NVS}$) and from the model only (A_{NVS}). The curves are calculations from [15] and [16].

5.3. Comparison with other existing measurements

For $Q^2 = 0.1$ (GeV/c)^2 the measurements from parity violation experiments can be regrouped for a better global determination of the strange form factors. The corresponding results are presented in Figure 14 together with theoretical predictions of [17], [18], [19] and [20]. The ellipses represent the 95.5% and 68.3% confidence level allowed by the data. The deduced final values are:

$$\boldsymbol{G_E^s\,(0.1) = -0.0130 +/- 0.028} \quad \text{and} \quad \boldsymbol{G_M^s(0.1) = 0.62 +/- 0.31}.$$

The theoretical approaches are not yet satisfactory, underestimating clearly the strange quark contribution to the magnetic properties of the proton ($\boldsymbol{G_M^s}$).

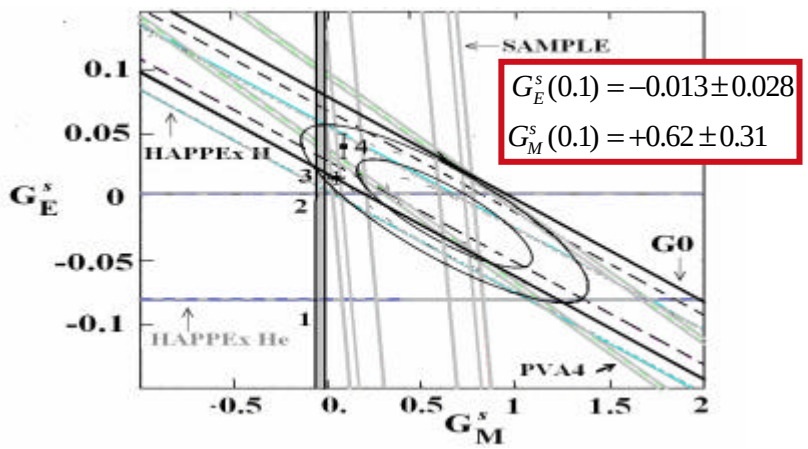

Figure 14. Experimental range for G_E^s and G_M^s from world data.
The numbers 1, 2, 3 and 4 refers to theoretical calculations o [17], [18], [19] and [20] respectively.

6. Future developments

6.1. Physics and content

The reason for the backward angle measurements is the separation of electric and magnetic form factors at different Q^2. As explained already, at one given angle from parity-violating asymmetries only a linear combination of electric, magnetic and axial form factors is accessed. To isolate each contribution it is necessary to do complementary measurements. They will be asymmetries from elastic electron scattering at a backward angle from both hydrogen and deuterium targets. Due to time limitation the proposal is restricted to 3 beam energies therefore to 3 different Q^2 values. To complement and compare with other experiments it is planned to explore successively three regions of Q^2 (exact values to be determined).

Apart of strange and axial form factors, additional physics information will be obtained from backward angle measurements. Concurrently with $\vec{e} + p$ elastic scattering, events corresponding to scattering in the $N \rightarrow \Delta$ region can be isolated and will give access to the $N \rightarrow \Delta$ axial transition form-factor $G^{ND}_A(Q^2)$, a first measurement in this neutral current process [21].

6.2. Experimental needs :

In the backward-angle mode, the magnet and detectors will be rearranged so that the detectors are upstream of the magnet and so that elastically scattered electrons can be detected. As elastic and inelastic electrons are not separable by the TOF technique, additional detectors must be inserted to define the trajectories of the electrons and to perform particle identification. A new plane of scintillators at the exit of the cryostat (CED's for Cryostat Exit Detectors) and an aerogel Cerenkov counter are inserted for each octant. Since TOF will not be useful, the experiment would be done at the usual CEBAF frequency of 499Hz and the beam intensity increase to 80 µA. New trigger and coincidence electronics are therefore required, and a new target too. This cryogenic target would be filled either by liquid hydrogen or deuterium for the full study of strange and axial form factors. The new set-up and results from simulations are shown in Figure 16.

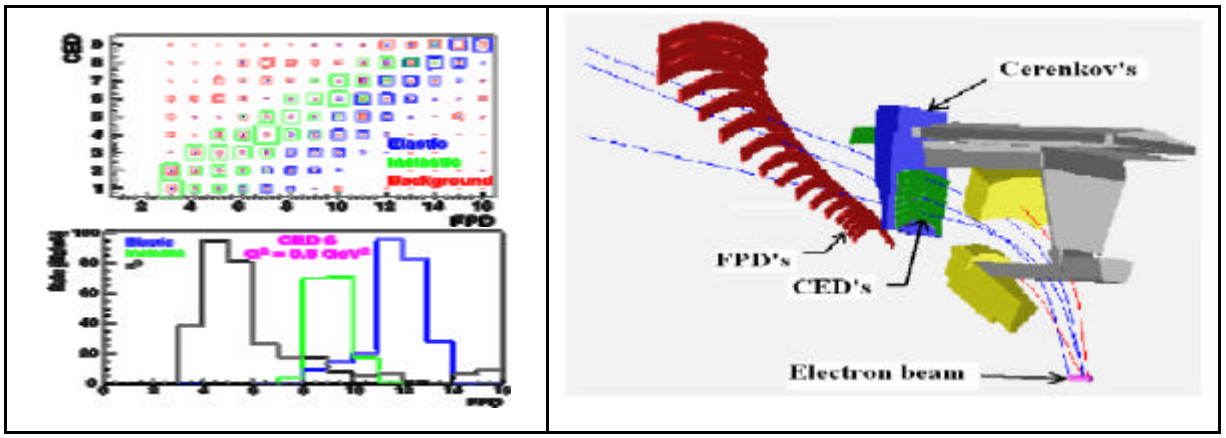

Figure 15: Backward angle set-up and simulation results.
An artist view shows the location of the new CED and Cerenkov detectors for one octant. The results of simulations on the left indicate the possible separation of elastic, inelastic and background events by mean of two-dimensional and one-dimensional plots.

The data taking campaign is planned from March to December 2006.

Conclusion

G0 is already a very productive experiment [22] that will only be completed with the backward angle measurements, giving coherent separation of the different form factors of the nucleon at the strange quark level over a large range of Q^2. This work is supported in part by CNRS (France), DOE (U.S.), NSERC (Canada) and NSF (U.S.) and benefits from strong technical contributions from many groups: Caltech, Illinois, LPSC-Grenoble, IPN-Orsay, TRIUMF and particularly the Accelerator and Hall C groups at Jefferson Lab.

The new results may be available within few years and will be worth a presentation in one of the next coming NUPPAC meetings.

References:

[1] Aniol,K.A. *et al*., Phys. Rev. **C70,** 065501 (2004) ; Aniol,K.A. *et al*., **nucl-ex/0506010**_; Aniol,K.A. *et al*., **nucl-ex/0506011**. {HAPPEX}

[2] Maas,F.E. *et al*., Phys. Rev.Lett. **93,** 022002 (2004); Maas,F.E. *et al*., Phys. Rev.Lett. **94,** 152001 (2005). {PVA4}

[3] Spayde,D.T. *et al*., Phys. Lett. **B583,** 79 (2004). {SAMPLE}

[4] Beck,D.H., spokesperson, *Measurement of the Flavor Singlet Charge Form Factor of the proton* G^0, Jefferson Lab proposal **PR91-017** and following **E00-006**, **E01-116, E04-101, E04-115** and **PR05-108 .** {G0}

[5] Armstrong,D.S. *et al*., Phys. Rev. Lett. **95,** 092001 (2005). {G0}

[6] Bimbot,L. for the G0 collaboration, " The G0 parity violation experiment: overview and status after the first commissioning run " , in *Proceedings of NUPPAC'O3*, Fayoum, Egypt October 11-15, 2003, Comsan,M.N.H. and Hanna,K.M. editors, 2005, pp 9-25.

[7] Beck,D.H. and McKeown,R.D. Ann. Rev. Nucl. Part. Sci. **51,** 189 (2001).

[8] Covrig,S. *et al*., submitted to N.I.M., **nucl-ex/0502019**.

[9] Real,J.S. http://g0web.jlab.org/analysislog/Analysis_Notes/106

[10] Liu,J. http://g0web.jlab.org/analysislog/Analysis_Notes/110

[11] Liu,J. http://g0web.jlab.org/analysislog/Analysis_Notes/111

[12] Liu,J. http://g0web.jlab.org/analysislog/Analysis_Notes/76

[13] Afanasev,A.V. *et al*., Phys. Lett. B **514,** 269 (2001) and Guler,H. Thesis, University Paris-Sud (2003), unpublished.

[14] Kelly,J.J., Phys. Rev. **C 70,** 068202 (2004).

[15] Arrington,J., Phys. Rev. **C 69,** 022201 (2004).

[16] Friedrich,J. and Walcher,T., Eur. Phys. J. **A.17,** 607 (2003).

[17] Leinweber,D.B. *et al*., Phys. Rev. Lett. **94,** 212001 (2005).

[18] Lyubovitskij,V.E. *et al*., Phys. Rev.**C 66,** 055204 (2002).

[19] Lewis,R. *et al*., Phys. Rev. **D 67,** 013003 (2003).

[20] Silva,A. *et al*., Phys. Rev. **D 65,** 014016 (2001).

[21] Wells,S.P. and Simicevic,N. spokespersons, Jefferson Lab. proposal **E01-115** (2001).

[22] http://focus.aps.org/story/v16/st7